Matter-Wave Interferometry Tests of Density Field Dynamics

Gary Alcock[1]

[1] *Independent Researcher, Los Angeles, CA, USA*

(Dated: September 18, 2025)

Density Field Dynamics (DFD) posits a scalar refractive field $\psi(\mathbf{x})$ such that light propagates with $n = e^{\psi}$ (ONE-WAY phase speed $c_1 = ce^{-\psi}$) and matter accelerates as $\mathbf{a} = \frac{c^2}{2}\nabla\psi$. While our cavity–atom redshift test probes the photon sector, *matter-wave interferometers* test the external wavefunction coupling. We derive the perturbative phase from the $\nabla\psi\cdot\nabla$ operator in the DFD-modified Schrödinger equation and obtain a clean discriminator for light-pulse interferometers:

$$\boxed{\Delta\phi_{\rm DFD} = \frac{\hbar\, k_{\rm eff}^2}{m}\,\frac{g}{c^2}\,T^3},$$

in contrast to the standard GR scaling $\Delta\phi_{\rm GR} = k_{\rm eff} g T^2$. We provide explicit, plug-in predictions for Kasevich–Chu, Raman, and Bragg geometries (vertical and horizontal), source-mass configurations, and dual-species protocols (Rb/Yb), and we analyze systematics with look-alike time scalings. For Earth g and $k_{\rm eff} \sim 1.6\times10^7\,\mathrm{m}^{-1}$ (Rb, 780 nm), the DFD residual is $\sim 2\times10^{-11}$ rad at $T = 1$ s, within the reach of current long-baseline instruments when using rotation, k-reversal, and source-mass modulation.

I. INTRODUCTION

Atom interferometers are leading probes of gravity, redshift, and fundamental symmetries.[1–6] In DFD, photons follow the eikonal of an optical metric with $n = e^{\psi}$ while matter sees the conservative potential $\Phi = -\frac{c^2}{2}\psi$.[1] The photon-sector discriminator is a co-located cavity–atom redshift comparison across altitude; here we develop the *matter-sector* analogue: light-pulse atom interferometry. The novelty is a gradient–gradient coupling that yields a T^3 scaling distinct from the GR T^2 law, giving a route to sector-resolved falsification with existing facilities.

Relation to existing gravity-gradient cancellation and why it was not seen. Long-baseline experiments *actively suppress or calibrate out* cubic-in-T gravity-gradient contributions using frequency-shift gravity-gradient (FSGG) compensation or closely related k-vector tuning schemes,[27–30] because within GR such terms are treated as *systematics*. As a result, published analyses typically (i) operate at fixed T for the headline measurement, (ii) do not report a residual *vs.* T regression with the *even-in-$k_{\rm eff}$*, rotation-odd discriminator posed here, and (iii) use k-reversal specifically to cancel odd-in-$k_{\rm eff}$ laser/systematic terms. To our knowledge, no experiment has isolated a coefficient $b_{\rm even}$ in $\phi_{\rm res}(T) = aT^2 + b_{\rm even}T^3$ that (a) is *even* under $k_{\rm eff}\to -k_{\rm eff}$ and (b) *flips sign* under 180° rotation of a horizontal baseline—the specific signature predicted here.

[1] See the Einstein 1911–12 completion and the strong-field/GW manuscripts for the action, normalization, and recovery of GR's weak-field coefficients; we adopt that notation here.

II. THEORY: ψ-COUPLING IN THE SCHRÖDINGER DYNAMICS

To first order in weak fields ($|\psi| \ll 1$), the nonrelativistic equation for mass m reads (expanding $e^{-\psi} \approx 1-\psi$)

$$i\hbar\,\partial_t\Psi = -\frac{\hbar^2}{2m}\nabla^2\Psi + m\Phi\,\Psi + \frac{\hbar^2}{2m}\Big[\psi\,\nabla^2\Psi + (\nabla\psi)\cdot\nabla\Psi\Big], \quad (1)$$

with $\Phi \equiv -\frac{c^2}{2}\psi$. Treat $H = H_0 + \delta H$ with $H_0 = \frac{p^2}{2m} + m\Phi$ and

$$\delta H = \frac{\hbar^2}{2m}\Big[\psi\,\nabla^2 + (\nabla\psi)\cdot\nabla\Big]. \quad (2)$$

Evaluate the small phase along the unperturbed classical branches A, B:

$$\Delta\phi_{\rm DFD} = \frac{1}{\hbar}\int_0^{2T} dt\,\Big(\langle\delta H\rangle_A - \langle\delta H\rangle_B\Big). \quad (3)$$

The operator $(\nabla\psi)\cdot\nabla$ acting on a locally plane-wave factor on each branch pulls down the instantaneous momentum, $\langle(\nabla\psi)\cdot\nabla\rangle \to i\,(\nabla\psi)\cdot\mathbf{p}/\hbar$, so that

$$\boxed{\Delta\phi_{\nabla\psi} = -\frac{1}{2m}\int_0^{2T} dt\,(\nabla\psi)\cdot\Delta\mathbf{p}(t)}. \quad (4)$$

In uniform Earth gravity, $\nabla\psi = -2\mathbf{g}/c^2$; the constant part cancels between arms unless one accounts for the *finite spatial separation* of the arms induced by the light pulses. Keeping the leading variation sampled at the arm positions yields the T^3 law below.

III. LIGHT-PULSE GEOMETRIES AND THE T^3 DISCRIMINATOR

Consider a vertical Kasevich–Chu sequence ($\pi/2$–π–$\pi/2$ at $t = \{0, T, 2T\}$) with effective Raman wavevector $k_{\text{eff}}\hat{z}$. Let the recoil velocity be $v_r = \hbar k_{\text{eff}}/m$. Between pulses, the branch momentum difference is piecewise constant: $\Delta p_z(t) = +\hbar k_{\text{eff}}$ for $0 < t < T$, and $-\hbar k_{\text{eff}}$ for $T < t < 2T$ (mirror swaps the arms). Using (4) with $\nabla\psi(\mathbf{r}_{A,B}, t) = -2\, g\, \hat{z}/c^2$ evaluated at the *arm locations* and expanding to first order in the instantaneous arm separation $\Delta z(t)$ (which is $v_r t$ on the first half and $v_r(2T-t)$ on the second), the constant part cancels but the linear piece adds over the two intervals, giving

$$\boxed{\Delta\phi_{\text{DFD}}^{Kasevich--Chu} = \frac{k_{\text{eff}}\, v_r\, g}{c^2}\, T^3 = \frac{\hbar\, k_{\text{eff}}^2}{m}\, \frac{g}{c^2}\, T^3}. \quad (5)$$

By contrast, the standard light-pulse phase from GR (after the usual laser phase bookkeeping) is

$$\boxed{\Delta\phi_{\text{GR}}^{Kasevich--Chu} = k_{\text{eff}}\, g\, T^2}. \quad (6)$$

Numerics (Rb, 780 nm): $k_{\text{eff}} \simeq 1.6 \times 10^{7}\ \text{m}^{-1}$, $v_r = \hbar k_{\text{eff}}/m \approx 1.2 \times 10^{-2}\ \text{m}\,\text{s}^{-1}$. For $T = 1$ s,

$$\Delta\phi_{\text{DFD}}^{Kasevich--Chu} \approx \frac{(1.6 \times 10^{7})(1.2 \times 10^{-2})(9.8)}{(3.0 \times 10^{8})^2} \simeq 2 \times 10^{-11}\ \text{rad}. \quad (7)$$

The absolute GR phase $k_{\text{eff}} g T^2 \sim 1.6 \times 10^{8}$ rad is removed by chirp/common-mode subtraction; the *residual* DFD term is what to search for, using scaling and sign tests below.

A. Horizontal baselines and rotation

For a horizontal Raman/Bragg baseline with separation direction $\hat{\mathbf{n}}$, Earth's field projects as $\mathbf{g}\cdot\hat{\mathbf{n}}$:

$$\Delta\phi_{\text{DFD}}^{\text{horiz}} = \frac{\hbar\, k_{\text{eff}}^2}{m}\, \frac{\mathbf{g}\cdot\hat{\mathbf{n}}}{c^2}\, T^3, \quad (8)$$

which *flips sign* under 180° rotation about the vertical. This provides a powerful discriminator from many systematics.

B. Source-mass configuration (tabletop)

Place a dense source mass (e.g. $\sim$500 kg W) at distance R producing $g_s = GM/R^2$. Then

$$\Delta\phi_{\text{DFD}}^{\text{src}} = \frac{\hbar\, k_{\text{eff}}^2}{m}\, \frac{g_s}{c^2}\, T^3 \times \mathcal{G}(\text{geometry}), \quad (9)$$

where $\mathcal{G}$ encodes near-field placement; lock-in by modulating the mass.

C. Dual-species protocol (Rb/Yb)

Because the DFD term scales as $\Delta\phi_{\text{DFD}} = (\hbar k_{\text{eff}}^2/m)\,(g/c^2)\,T^3$, the differential phase between two species i, j operated in matched geometry is

$$\Delta\phi_{\text{DFD}}^{(i-j)} = \frac{g\, T^3}{c^2}\, \hbar \left(\frac{k_{\text{eff},i}^2}{m_i} - \frac{k_{\text{eff},j}^2}{m_j} \right). \quad (10)$$

If both species share the *same* lattice/Bragg wavelength (engineered co-propagating optics), $k_{\text{eff},i} = k_{\text{eff},j}$ and (10) reduces to a clean mass discriminator $\propto (1/m_i - 1/m_j)$. With independent Raman pairs (e.g. ^{87}Rb at 780 nm and ^{171}Yb at 556 nm), keep the explicit k_{eff} values; Eq. (10) is then the quantity to regress against T^3. In either case, the GR common-mode $k_{\text{eff}} g T^2$ cancels under standard k-reversal and conjugate-AI subtraction.

IV. CONCRETE EXPERIMENTAL DESIGNS (PLUG-AND-PLAY)

Design A (vertical Kasevich–Chu, 10 m fountain). Species ^{87}Rb, $\lambda = 780$ nm, $k_{\text{eff}} \approx 1.6 \times 10^{7}\ \text{m}^{-1}$, pulses at $t = \{0, T, 2T\}$ with $T = 1$–2 s. Arm apex separation $\Delta z_{\text{max}} \approx v_r T \sim 1$–$2$ cm.

$$\Delta\phi_{\text{DFD}} \approx 2 \times 10^{-11}\ \text{rad} \times (T/\text{s})^3.$$

Design B (horizontal Bragg, $L \sim 1$ m, rotation). Rotate the bench by 180° about $\hat{z}$ to flip $\mathbf{g}\cdot\hat{\mathbf{n}}$. DFD flips sign; many laser/system alignment systematics do not.

Design C (tabletop source mass). Dither a 500 kg tungsten stack at $R \sim 0.25$ m. Search at the dither frequency; scale with g_s/c^2.

V. DISCRIMINANTS FROM GR AND SYSTEMATICS CONTROL

Key orthogonal signatures:

1. **Time scaling:** DFD $\propto T^3$ vs. GR $\propto T^2$.
2. **Orientation:** rotation flips DFD (via $\mathbf{g}\cdot\hat{\mathbf{n}}$), many systematics do not.
3. **k-reversal:** DFD $\propto k_{\text{eff}}^2$ (even under $k_{\text{eff}} \to -k_{\text{eff}}$); laser-phase systematics change sign and cancel.
4. **Recoil dependence:** DFD $\propto v_r$; separate from gravity-gradient terms using velocity selection.
5. **Dual-species:** residual $\propto (1/m_1 - 1/m_2)$ or the full k_{eff}^2/m contrast in Eq. (10); GR null after common-mode rejection.

Systematics evidence and controls. Gravity-gradient noise (GGN) from atmosphere and seismic fields sets the long-baseline floor; recent characterizations provide

TABLE I. Systematics overview and kill-switches. The DFD signal alone shows T^3 scaling, rotation sign flip, and even parity under k-reversal ($\propto k_{\rm eff}^2$).

Effect	T-scaling	Rotation flip	k-reversal parity
DFD (target)	T^3	Yes	Even ($k_{\rm eff}^2$)
Gravity gradient Γ	T^2/T^3 mix	Often No	Mixed
Wavefront curvature / tilt	T^2	No	Odd (cancels)
Vibrations (residual)	$\approx T^2$	No	Odd/Even mix
AC Stark / Zeeman	pulse-bounded	No	Design-dependent
Laser phase (uncorrelated)	T^2	No	Odd (cancels)

high/low-noise models and motivate underground siting or subtraction.[20, 21] Wavefront aberrations are a leading accuracy term; dedicated measurements and in-situ phase-retrieval methods demonstrate $< 3\times10^{-10}\,g$ equivalent bias and routes to further reduction.[18, 19] Active isolation routinely delivers 10^2–10^3 vertical attenuation at 30 mHz–10 Hz in fieldable systems.[14] Frequency-dependent electronics/Raman-chirp phases are odd-in-$k_{\rm eff}$ and cancel under k-reversal with residuals characterized and mitigated.[17, 24] Rotation platforms and mirror-tilt compensation explicitly separate Coriolis/Sagnac terms and have been demonstrated across wide orientation/rotation ranges.[15, 23] Source-mass gravity signals in horizontal/baseline geometries establish lock-in protocols directly applicable to our T^3 search.[22]

VI. SENSITIVITY SNAPSHOT AND FEASIBILITY

Long-baseline results demonstrate the needed stability and controls: the Stanford 10 m fountain achieved long-time point-source interferometry with single-shot acceleration sensitivity at the few$\times10^{-9}\,g$ level and 1.4 cm arm separation,[7, 8] while dual-species EP tests reached $\eta \sim 10^{-12}$ with $2T = 2\,$s free fall.[9] VLBAI (Hannover) reports high-flux Rb/Yb sources, 10 m magnetic shielding, and seismic attenuation tailored for long baseline.[10, 11] SYRTE's absolute gravimeters and mobile surveys document μGal-class stability with active vibration isolation.[12–14] These capabilities jointly bound key systematics (vibration, wavefronts, gradients) at or below our target $|\Delta\phi_{\rm DFD}| \sim 2\times10^{-11}\,$rad for $T \sim 1\,$s, and several groups already deploy rotation control and k-reversal protocols routinely.[15–17]

VII. DISCUSSION AND OUTLOOK

This work closes the *matter-sector* gap in the DFD experimental program. Together with the cavity–atom redshift comparison (photon sector), matter-wave tests over-constrain the sector coefficients. A null result at or below the $|\Delta\Phi|/c^2$ lever arm (after the stated controls) would falsify this DFD sector. Positive detection would present a geometry-locked, scaling-locked deviation from GR that cannot be attributed to standard systematics.

ACKNOWLEDGMENTS

I thank colleagues in precision atom interferometry for advice on rotation tests, dual-species protocols, and source-mass lock-in strategies.

Appendix A: Sketch of the T^3 derivation from the gradient operator

Write the branch centers as $z_{A,B}(t) = z_0(t) \pm \frac{1}{2}\Delta z(t)$ with $\Delta z(t) = v_r t$ for $0 < t < T$ and $\Delta z(t) = v_r(2T - t)$ for $T < t < 2T$. Expand the field along the arms:

$$\nabla\psi(z_{A,B}) \approx \nabla\psi(z_0) \pm \tfrac{1}{2}\Delta z\,\partial_z(\nabla\psi)|_{z_0}. \tag{A1}$$

The constant part $\nabla\psi(z_0)$ cancels in (4) because $\int_0^{2T}\Delta p_z\,dt = 0$ for the piecewise $\pm\hbar k_{\rm eff}$ profile. The linear term gives (using Earth field $\partial_z(\nabla\psi) = -2\Gamma\,\hat{z}/c^2$ and the kinematic separation implicit in Δz)

$$\begin{aligned}\Delta\phi_{\nabla\psi} &= -\frac{1}{2m}\int dt\,\left[\tfrac{1}{2}\Delta z(t)\,\partial_z(\nabla\psi)\right]\cdot\Delta\mathbf{p}(t)\\ &\to \frac{g}{c^2}\frac{\hbar k_{\rm eff}}{m}\int_0^T t\,dt \;+\; \frac{g}{c^2}\frac{\hbar k_{\rm eff}}{m}\int_T^{2T}(2T-t)\,dt\\ &= \frac{\hbar k_{\rm eff}}{m}\frac{g}{c^2}\Big(\frac{T^2}{2}+\frac{T^2}{2}\Big)T = \frac{\hbar k_{\rm eff}}{m}\frac{g}{c^2}T^3, \end{aligned} \tag{A2}$$

and multiplying by the impulsive momentum separation $\hbar k_{\rm eff}$ from the light pulses yields (5). A full WKB treatment gives the same result and shows cancellation of the companion $\psi\nabla^2$ piece for these geometries.

Appendix B: Figure templates (TikZ/PGFPlots)

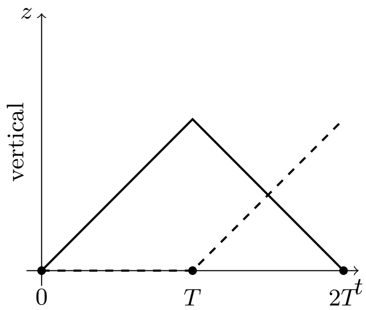

FIG. 1. Light-pulse Mach–Zehnder (Kasevich–Chu) geometry. Solid/dashed are the two arms; pulses at $0, T, 2T$.

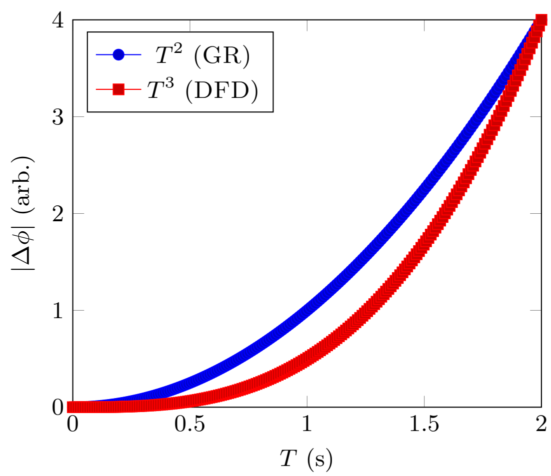

FIG. 2. Scaling discriminator: DFD T^3 vs. GR T^2.

[1] M. Kasevich and S. Chu, "Measurement of the gravitational acceleration of an atom with a light-pulse interferometer," *Appl. Phys. B* **54**, 321 (1992).

[2] A. Peters, K. Y. Chung, and S. Chu, "High-precision gravity measurements using atom interferometry," *Metrologia* **38**, 25 (2001).

[3] S. Dimopoulos, P. W. Graham, J. M. Hogan, and M. A. Kasevich, "Atomic gravitational wave interferometric sensor," *Phys. Rev. D* **78**, 122002 (2008).

[4] G. M. Tino and M. A. Kasevich (eds.), *Atom Interferometry* (IOS Press, 2014).

[5] A. D. Cronin, J. Schmiedmayer, and D. E. Pritchard, "Optics and interferometry with atoms and molecules," *Rev. Mod. Phys.* **81**, 1051 (2009).

[6] J. M. Hogan, D. M. S. Johnson, and M. A. Kasevich, "Atom interferometry," *Nat. Phys.* **16**, 913 (2020).

[7] S. M. Dickerson *et al.*, "Multiaxis Inertial Sensing with Long-Time Point Source Atom Interferometry," *Phys. Rev. Lett.* **111**, 083001 (2013).

[8] A. Sugarbaker *et al.*, "Enhanced Atom Interferometer Readout through the Application of Phase Shear," *Phys. Rev. Lett.* **111**, 113002 (2013).

[9] P. Asenbaum *et al.*, "Atom-Interferometric Test of the Equivalence Principle at the 10^{-12} Level," *Phys. Rev. Lett.* **125**, 191101 (2020).

[10] D. Schlippert *et al.*, "Very long baseline atom interferometry," Proc. SPIE (2024).

[11] D. Schlippert *et al.*, "The Hannover Very Long Baseline Atom Interferometer," APS DMP (2022).

[12] P. Gillot *et al.*, "The LNE–SYRTE cold atom gravimeter," LNE–SYRTE report (2015).

[13] X. Wu *et al.*, "Gravity surveys using a mobile atom interferometer," *Sci. Adv.* **5**, eaax0800 (2019).

[14] F. E. Oon *et al.*, "Compact active vibration isolation and tilt stabilization for a transportable quantum gravimeter," *Phys. Rev. Applied* **18**, 044037 (2022).

[15] Q. d'Armagnac de Castanet *et al.*, "Atom interferometry at arbitrary orientations and rotation rates," *Nat. Commun.* **15**, 6080 (2024).

[16] D. Yankelev *et al.*, "Atom interferometry with thousand-fold increase in dynamic range," *PNAS* **117**, 23414 (2020).

[17] B. Cheng *et al.*, "Influence of chirping the Raman lasers in an atom gravimeter," *Phys. Rev. A* **92**, 063617 (2015).

[18] V. Schkolnik *et al.*, "The effect of wavefront aberrations in atom interferometry," *Appl. Phys. B* **120**, 311 (2015).

[19] W. J. Xu *et al.*, "In situ measurement of the wavefront phase shift in an atom interferometer," *Phys. Rev. Applied* **22**, 054014 (2024).

[20] J. Carlton *et al.*, "Characterizing atmospheric gravity gradient noise for vertical atom interferometers," *Phys. Rev. D* **111**, 082003 (2025).

[21] J. Carlton *et al.*, "Clear skies ahead: atmospheric gravity gradient noise for vertical atom interferometers," arXiv:2412.05379 (2024).

[22] G. W. Biedermann *et al.*, "Testing gravity with a horizontal gravity-gradiometer atom interferometer," *Phys. Rev. A* **91**, 033629 (2015).

[23] Q. Beaufils *et al.*, "Rotation-related systematic effects in a cold atom accelerometer on a satellite," *NPJ Microgravity* **9**, 37 (2023).

[24] Y. Xu *et al.*, "Evaluation of a frequency-dependent phase shift in chirped-Raman atom gravimeters," *Phys. Rev. A* **110**, 062816 (2024).

[25] D. Schlippert *et al.*, "Quantum Test of the Universality of Free Fall Using Rubidium and Potassium," *Phys. Rev. Lett.* **112**, 203002 (2014).

[26] C. Overstreet *et al.*, "Observation of effective field theory effects in atom interferometry," *Science* **375**, 226 (2022).

[27] G. D'Amico, G. Rosi, S. Zhan, L. Cacciapuoti, M. Fattori, and G. M. Tino, "Canceling the Gravity Gradient Phase Shift in Atom Interferometry," *Phys. Rev. Lett.* **119**, 253201 (2017).

[28] C. Overstreet, P. Asenbaum, T. Kovachy, R. Notermans, J. M. Hogan, and M. A. Kasevich, "Effective Inertial Frame in an Atom Interferometric Test of the Equivalence Principle," *Phys. Rev. Lett.* **120**, 183604 (2018).

[29] A. Roura, "Circumventing Heisenberg's Uncertainty Principle in Atom Interferometry Tests of the Equivalence Principle," *Phys. Rev. Lett.* **118**, 160401 (2017).

[30] P. Asenbaum, C. Overstreet, T. Kovachy, D. D. Brown, J. M. Hogan, and M. A. Kasevich, "Phase Shift in an Atom Interferometer due to Spacetime Curvature across its Wave Function," *Phys. Rev. Lett.* **118**, 183602 (2017).